Quantum Electronics **51** (2) 158–163 (2021)
©2021 Kvantovaya Elektronika and IOP Publishing Limited

GENERATION OF TERAHERTZ RADIATION
https://doi.org/10.1070/QEL17461

THz laser generation on a hybrid surface plasmon in a HgCdTe-based structure

A.A. Dubinov, V.Ya. Aleshkin, V.I. Gavrilenko, V.V. Rumyantsev, N.N. Mikhailov, S.A. Dvoretskii, V.V. Utochkin, S.V. Morozov

***Abstract.* The possibility of amplifying a THz hybrid surface plasmon in a structure with an $Hg_{0.82}Cd_{0.18}Te$ epitaxial film grown on a GaAs substrate and covered with a metal layer is investigated. It is shown that for a film thickness of 100 nm and a temperature of 80 K, the hybrid surface plasmon mode gain can be greater than external losses at a pump radiation intensity with a wavelength of 2.3 μm, exceeding 850 kW cm^{-2}. Additional doping of the $Hg_{0.82}Cd_{0.18}Te$ layer with a donor impurity having a concentration of 4×10^{17} cm^{-3} will lead to a 1.5-fold decrease in the threshold pump intensity.**

Keywords: *hybrid plasmon, terahertz radiation, laser.*

1. Introduction

At present, monopolar quantum cascade lasers (QCLs) based on III–V compounds take the leading place among semiconductor radiation sources in the THz frequency range. However, there is a frequency range (6–15 THz), in which the operation of these QCLs is difficult and often impossible due to a strong absorption of laser radiation by polar optical phonons [1]. Materials for which the frequencies of polar optical phonons are located far from the frequency range in question can serve as an alternative to III–V materials. Such a material, in particular, is the HgCdTe (mercury cadmium telluride, MCT) solid solution, whose optical phonons have frequencies in the 4-THz region. This material is widely used to manufacture mid-IR detectors and detector arrays (see, for example, work [2] and references therein). On the other hand, it has recently been proposed to use quantum wells based on HgCdTe to produce a QCL generating radiation at frequencies of ~8.3 THz [3].

However, QCLs, including those based on HgCdTe, are rather difficult to fabricate due to the need to grow a huge number of quantum-well layers of the required quality. Therefore, an alternative to amplification at intersubband optical transitions (as in QCLs) can be amplification at interband optical transitions in the THz frequency range. To this end, it is advisable to use structures based on HgCdTe, in which the band gap can be varied within wide limits (from zero to 1.6 eV) by changing the fraction of Cd [2].

Optically pumped mid-IR interband lasers based on HgCdTe have been known for a long time [4]. Until recently, such lasers generated radiation only at frequencies exceeding 56 THz [5]. A significant progress in the technology of molecular beam epitaxy of such structures, achieved in recent years in a number of technological groups, opens up broad prospects for the fabrication of THz radiation sources, which is demonstrated by the latest published experimental results. In particular, in laser structures based on interband transitions with 10 HgTe/HgCdTe quantum wells, stimulated emission was observed for the first time under optical pumping at frequencies in the 15-THz region [6, 7].

When HgTe/HgCdTe quantum wells are used instead of bulk HgCdTe layers as an active medium, the Auger recombination rate is significantly reduced [6, 8, 9], which, as shown by theoretical estimates [10], will make it possible to generate radiation at frequencies slightly exceeding 5 THz at temperatures below the temperature of liquid nitrogen. However, the estimates of the lasing threshold made in [10] (the intensity of pump radiation with a wavelength of 2.15 μm was 10–100 kW cm^{-2}) for the frequency range from 5 to 15 THz are not entirely correct, since the characteristics of waveguide modes in laser (absorption in passive layers α_p, losses on mirrors α_m, and optical confinement factor Γ) were not calculated. In fact, Alymov et al. [10] calculated the transparency thresholds at which the gain of the active medium G becomes equal to its absorption coefficient α_a, rather than the lasing thresholds $[(G - \alpha_a)\Gamma = \alpha_p + \alpha_m]$. If Drude absorption at the laser radiation frequency in its passive undoped layers can be neglected when choosing an optical pump quantum energy smaller than the band gap of these layers (absorption of pump radiation only in the active medium), then phonon absorption in HgCdTe solutions cannot be neglected. It also becomes important to take into account the absorption of radiation by phonons in the above frequency range in the GaAs substrate, which is used to grow laser structures based on HgCdTe [6–8]. Previous calculations showed [11] that the coefficient of this absorption can be ~20 cm^{-1}, and the optical confinement factor for the fundamental TE mode of a dielectric waveguide in a struc-

A.A. Dubinov Institute for Physics of Microstructures, Russian Academy of Sciences, GSP-105, 603950 Nizhny Novgorod, Russia; Lobachevsky State University of Nizhny Novgorod, prosp. Gagarina 23, 603950 Nizhny Novgorod, Russia;
e-mail: sanya@ipm.sci-nnov.ru;
B.Ya. Aleshkin, V.I. Gavrilenko, V.V. Rumyantsev, V.V. Utochkin, S.V. Morozov Institute for Physics of Microstructures, Russian Academy of Sciences, GSP-105, 603950 Nizhny Novgorod, Russia;
N.N. Mikhailov, S.A. Dvoretskii Rzhanov Institute of Semiconductor Physics, Siberian Branch, Russian Academy of Sciences, prosp. Akad. Lavrent'eva 13, 630090 Novosibirsk, Russia

Received 7 October 2020
Kvantovaya Elektronika **51** (2) 158–163 (2021)
Translated by I.A. Ulitkin

ture with five $HgTe/Hg_{0.3}Cd_{0.7}Te$ quantum wells is ~0.004. Therefore, for lasing to appear, the difference $G - \alpha_a$ should exceed 5000 cm^{-1}.

The optical confinement factor and, accordingly, the mode gain ($g = G\Gamma$) can be significantly higher when a two-dimensional plasmon, rather than the TE mode, is excited, which is one of two TM modes localised near a quantum well with a sufficient concentration of free carriers [12]. In a two-dimensional plasmon propagating in the direction of the x axis, there are two components of the electric field. The component of the electric field $E_x(z)$ is symmetric about the z axis that is perpendicular to the plane of the quantum well, if the middle of the well is chosen as point $z = 0$, i.e., $E_x(z) = E_x(-z)$. The second component $E_z(z)$ is antisymmetric, i.e., $E_z(z) = -E_z(-z)$. The effective refractive index of this mode, $n_{\rm eff}$, exceeds 100; therefore, it is rather difficult to match it with the open-space modes. To efficiently outcouple radiation of such a mode from the structure, it is necessary, for example, to apply a metal grating with a period on the order of $\lambda/n_{\rm eff}$ to the structure, where λ is the radiation wavelength in vacuum.

Another TM mode, the electric field component $E_z(z)$ of which is symmetric in the quantum well, and the electric field component $E_x(z)$ is antisymmetric, is weakly localised near the quantum well. However, the component $E_z(z)$ can be strongly localised in the layer, whose modulus of the dielectric constant $|\varepsilon|$ is much less (or even close to zero) than the modulus of the dielectric constant of the medium surrounding this layer, since the following boundary condition is valid for the TM mode: continuity of $E_z(z)/\varepsilon(z)$ at all boundaries. Materials with $|\varepsilon|$ close to zero (epsilon near zero materials, ENZ materials) possess unusual properties that can be realised in semiconductors at frequencies close to the plasma frequency [13, 14]. Surface plasmons propagating along the metal–ENZ material–ordinary material interfaces are called hybrid [15, 16].

It is known that the ground level of holes in HgTe/HgCdTe quantum wells is represented mainly by the states of heavy holes. Therefore, according to the selection rules for electron transitions between the valence and conduction bands [17], it is possible to amplify only those modes for which the component of the electric field lies in the plane of the quantum well and is symmetric with respect to it. Only TE modes and a two-dimensional plasmon have such a component of the electric field. In a bulk semiconductor, the valence band ceiling is degenerate: The energies of heavy and light holes coincide, and it is possible to amplify modes whose electric field component has an arbitrary direction. In the present work, we investigated the possibility of amplifying a hybrid surface plasmon in a structure based on a thin bulk $Hg_{0.82}Cd_{0.18}Te$ layer covered with a metal layer. This choice of the cadmium fraction in the solid solution is due to the fact that the band gap of the $Hg_{0.82}Cd_{0.18}Te$ (E_g) material is 44 meV (10.64 THz) at a temperature of 80 K [2], i.e., the radiation frequency falls into the range of interest.

Refractive indices $n_{\rm eff}$, Drude and phonon losses, and the amplification of the second considered TM mode were calculated. It was shown that at realistic parameters of the $Hg_{0.82}Cd_{0.18}Te/CdTe/GaAs$ structure and at a temperature close to the temperature of liquid nitrogen, the hybrid surface plasmon mode amplification can exceed external losses at a concentration of photoexcited carriers above 4.9×10^{17} cm^{-3}. And due to the doping of the $Hg_{0.82}Cd_{0.18}Te$ layer by donors with a concentration of 4×10^{17} cm^{-3}, it was possible to decrease the threshold concentration of photoexcited carriers to 2.2×10^{17} cm^{-3}.

2. Calculation of the dielectric constant

To calculate the characteristics of a hybrid surface plasmon in the frequency range of interest, it is necessary to know the frequency dependences of the complex dielectric constants of the structure layers (GaAs substrate, CdTe buffer layer, active $Hg_{0.82}Cd_{0.18}Te$ layer, Au layer), which can be experimentally implemented (see, for example, [6–8]). In addition, it is necessary to know the dependence of the dielectric constant of the $Hg_{0.82}Cd_{0.18}Te$ layer on the concentration of charge carriers. However, the literature lacks data on measurements of the real part of the dielectric constant (or refractive index) of this compound. One can only find experimental data on the absorption coefficient α (and the imaginary part of the refractive index n, since $\alpha = 2\omega {\rm Im}\, n/c$, where ω is the cyclic frequency, and c is the speed of light in vacuum) associated with interband transitions, which are sufficiently well approximated by the formula [18]:

$$\alpha(\omega) = K\frac{(\hbar\omega - E_g)^P}{\hbar\omega}, \quad (1)$$

where $\hbar$ is Planck's constant; α is measured in cm^{-1}; $\hbar\omega$ and E_g are taken in eV; $K = -20060 + 115750x + 32.43T - 64170x^2 + 0.43231T^2 - 101.92xT$; $P = 0.74487 - 0.44513x + (0.000799 - 0.000757x)T$; x is the fraction of cadmium in the solution; and T is the temperature in Kelvin.

According to [19], the dielectric constant of a narrow-gap $Hg_{1-x}Cd_xTe$ solution can be presented as a sum:

$$\varepsilon = \varepsilon_\infty + \Delta\varepsilon_{\rm inter} + \Delta\varepsilon_{\rm intra} + \Delta\varepsilon_{\rm ph}, \quad (2)$$

where $\varepsilon_\infty = 15.2 - 15.6x + 8.2x^2$ [2]; $\Delta\varepsilon_{\rm inter}$ and $\Delta\varepsilon_{\rm intra}$ are the parts of the dielectric constant associated with interband and intraband transitions, respectively; and $\Delta\varepsilon_{\rm ph}$ is the part of the dielectric constant associated with optical phonons. The term $\Delta\varepsilon_{\rm ph}$ in our frequency range (frequencies above 10 THz) can be neglected, since the frequencies of the optical phonons of the HgCdTe material lie in the region of 4 THz [2].

The part of the dielectric constant associated with intraband transitions can be represented in the form [19]

$$\Delta\varepsilon_{\rm intra} = -\frac{\omega_e^2\varepsilon_\infty}{\omega^2 + i\gamma_e\omega} - \frac{\omega_h^2\varepsilon_\infty}{\omega^2 + i\gamma_h\omega}, \quad (3)$$

where $\gamma_{e,h} = q/(m^*_{e,h}\mu_{e,h})$; q is the electron charge; $\omega^2_{e,h} = 4\pi N \times q^2/(m^*_{e,h}\varepsilon_\infty)$, $\mu_{e,h}$, and $m^*_{e,h}$ are the square of the plasma frequency, mobility, and effective masses of conduction of electrons (e) and holes (h), respectively; and N is the carrier concentration (the same for electrons and holes under optical pumping). The mobility of electrons at temperatures below 100 K and for electron concentrations below 10^{18} cm^{-3} can be considered to be equal to

10^5 cm^2 V^{-1} s^{-1} [20], and the hole mobility under the same conditions is ~350cm^2 V^{-1} s^{-1} [2].

The spectra of electrons and light holes in bulk narrow-gap HgCdTe solutions are nonparabolic [19]:

$$E_{\rm e,lh}(k) = \frac{1}{2}\left(\pm\sqrt{E_{\rm g}^2 + \frac{2\hbar^2k^2E_{\rm g}}{m_{\rm e}}} + E_{\rm g}\right), \tag{4}$$

where $E_{\rm e}(k)$ and $E_{\rm lh}(k)$ are the energies of electrons [the plus sign in (4)] and light holes (the minus sign), respectively; k is the modulus of the wave vector; $m_{\rm e}$ is the effective mass of an electron; $m_{\rm e}/m_0 \approx 0.071E_{\rm g}$ ($E_{\rm g}$ is measured in eV); and m_0 is the mass of a free electron [2]. Therefore, $m_{\rm e}^*$ will depend on the electron concentration and temperature [21]:

$$m_{\rm e}^* = m_{\rm e} \times \frac{\int_0^\infty f_{\rm e}(E)(1+2E/E_{\rm g})\sqrt{E+E^2/E_{\rm g}}\,{\rm d}E}{\int_0^\infty f_{\rm e}(E)\sqrt{E+E^2/E_{\rm g}}\frac{1+[8E/(3E_{\rm g})](1+E/E_{\rm g})}{(1+2E/E_{\rm g})^2}{\rm d}E}, \tag{5}$$

where

$$f_{\rm e}(E) = \left[1+\exp\left(\frac{E-F_{\rm e}}{k_{\rm B}T}\right)\right]^{-1};$$

and $k_{\rm B}$ is the Boltzmann constant. The energy of the nonequilibrium quasi-Fermi level of electrons, $F_{\rm e}$, can be obtained from the expression relating N and $f_{\rm e}$:

$$N = \frac{1}{\pi^2}\int_0^\infty f_{\rm e}(E_{\rm e}(k))k^2{\rm d}k. \tag{6}$$

Using relation (5), we can find that in the $\rm Hg_{0.82}Cd_{0.18}Te$ layer at T = 80 K, the mass $m_{\rm e}^*$ will increase from $0.0082m_0$ to $0.032m_0$ when N changes from 10^{16} to 10^{18} cm^{-3}.

Because the density of states in the band of heavy holes is much higher than the density of states in the band of light holes, and hence their concentration is also higher, $m_{\rm h}^*$ will be determined only by the mass of heavy holes (the dispersion law for which is parabolic): $m_{\rm h}^* \approx m_{\rm hh} = 0.55m_0$ [2]. Hence it follows that at equal concentrations of electrons and holes, $\omega_{\rm e} \gg \omega_{\rm h}$ and only electrons will make the main contribution to $\Delta\varepsilon_{\rm intra}$.

Having determined from expression (1) the imaginary part of the dielectric constant associated with interband transitions, one can obtain from the Kramers–Kronig relations the real part of the corresponding dielectric constant [19]:

$${\rm Re}\Delta\varepsilon_{\rm inter} = \frac{c^2}{\pi^2}\left[\int_0^\infty \frac{{\rm d}A(\omega')}{{\rm d}\omega'}\lg\left(\frac{\omega'+\omega}{\omega'-\omega}\right){\rm d}\omega'\right]^2, \tag{7}$$

where

$$A(\omega) = \alpha(\omega)\left[f\left(\frac{(E_{\rm g}-\hbar\omega)/2-F_{\rm h}}{k_{\rm B}T}\right) - f\left(\frac{(\hbar\omega+E_{\rm g})/2-F_{\rm e}}{k_{\rm B}T}\right)\right];\quad f(x) = (1+\exp x)^{-1}.$$

The energy of the quasi-Fermi level of holes, $F_{\rm h}$, can be found from the expressions, which depend on the hole concentration N:

$$N = \frac{1}{\pi^2}\left[\int_0^\infty f_{\rm h}(E_{\rm hh}(k))k^2{\rm d}k + \int_0^\infty f_{\rm h}(E_{\rm lh}(k))k^2{\rm d}k\right],$$

$$f_{\rm h}(E) = \left[1+\exp\left(\frac{F_{\rm h}-E}{k_{\rm B}T}\right)\right]^{-1},\quad E_{\rm hh}(k) = -\frac{\hbar^2k^2}{2m_{\rm hh}}. \tag{8}$$

Using the above formulae for determining the dielectric constant of the $\rm Hg_{0.82}Cd_{0.18}Te$ layer, it is possible to plot the frequency dependence of the refractive index modulus of the material in question ($n_{\rm MCT} = \sqrt{\varepsilon}$) at various concentrations of photoexcited carriers in the frequency range of interest (see Fig. 1).

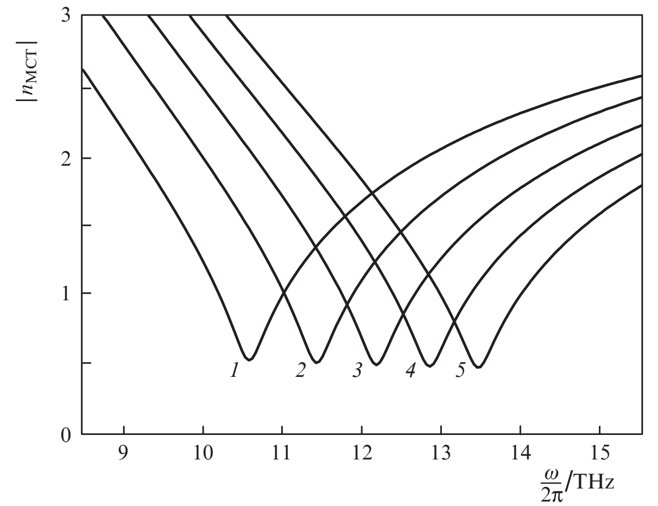

Figure 1. Frequency dependences of the refractive index modulus of the $\rm Hg_{0.82}Cd_{0.18}Te$ solution at T = 80 K for the concentrations of nonequilibrium carriers N = (*1*) 4×10^{17}, (*2*) 5×10^{17}, (*3*) 6×10^{17}, (*4*) 7×10^{17}, and (*5*) 8×10^{17} cm^{-3}.

Figure 1 shows that for each concentration there is a resonance frequency at which $|n_{\rm MCT}|$ takes the minimum value. For the parameters we have chosen, this value is close to 0.5, which is much less than $\sqrt{\varepsilon_\infty}$. Therefore, at such resonance frequencies, $\rm Hg_{0.82}Cd_{0.18}Te$ can be considered an ENZ material. It is also seen from Fig. 1 that the resonant frequency also increases with increasing N.

The dielectric constant of undoped wide-gap CdTe and GaAs semiconductors in the THz range was calculated by the formula from [22] using experimental data for GaAs [22] and CdTe [23]:

$$\varepsilon_j(\nu) = \varepsilon_{\infty j} + \frac{S_j^2}{\nu_{{\rm TO}j}^2 - \nu^2 + {\rm i}\delta_j\nu}, \tag{9}$$

where j = 1 corresponds to CdTe, and j = 2 to GaAs; $\nu = \omega/2\pi$; $\varepsilon_{\infty 1}$ = 8.52; $\varepsilon_{\infty 2}$ = 11.1; S_1 = 8.171 THz; S_2 = 11.392 THz; $\nu_{\rm TO1}$ = 4.248 THz; $\nu_{\rm TO2}$ = 8.055 THz; δ_1 = 259 GHz; and δ_2 = 72 GHz. To calculate the dielectric constant of Au, we used data interpolation from the reference book [24].

3. Amplification of a hybrid surface plasmon

We will use the following structure: A 5-μm-thick CdTe buffer layer (the minimum thickness required for the growth of a high-quality HgCdTe layer on it [25]) was grown on a GaAs substrate (for simplicity, it is considered to be semi-infinite), and then an active $Hg_{0.82}Cd_{0.18}Te$ layer with a thickness of $d = 100$ nm was grown (at this thickness, dimensional quantisation can be neglected, and the distribution of photoexcited carriers will be uniform, because $\alpha \approx 10^4$ cm^{-1} for pump frequencies corresponding to the mid- and near-IR wavelength ranges [26]), followed by a 50-nm-thick limiting CdTe layer (protecting the structure from surface nonradiative recombination of carriers) separating the active region from the metal (Au).

The components of the magnetic field H_y and the electric field E_x, E_z in the TM mode propagating along the structure described above, as well as the real part of the effective refractive index Re$n_{\rm eff}$ and the effective absorption coefficient $\alpha_{\rm eff}$ can be found by solving Maxwell's equations [27]. Note that $\alpha_{\rm eff}$ takes into account absorption in all layers of the structure. As an example, Fig. 2 shows the frequency dependences of Re$n_{\rm eff}$ and $\alpha_{\rm eff}$ at $N = 5\times10^{17}$ cm^{-3}. One can see that these values have maxima at close frequencies, and the maximum $\alpha_{\rm eff}$($\sim$4000 cm^{-1}) is rather sharp. When the frequency tends to the frequency corresponding to the minimum of $|n_{\rm MCT}|$, the mode disappears, i.e. it ceases to be localised. This is confirmed by Fig. 3, which shows the dependences of the squared modulus $E_z(z)$. The calculation shows that at a frequency of 10 THz, the jump $|E_z(z)|^2$ at the CdTe–$Hg_{0.82}Cd_{0.18}Te$ interface is small (by a factor of 3.9), because $|n_{\rm CdTe}|/|n_{\rm MCT}| = 2.776/1.974$, but the mode is rather strongly localised (the localisation region is $\sim$10 mm), and therefore such an important parameter as the optical confinement factor Γ [28] is 0.088. In this case, $\alpha_{\rm eff}$ = 77 cm^{-1}, and the gain $G = -A(\omega)$ in the $Hg_{0.82}Cd_{0.18}Te$ layer at this frequency is still negative, because the frequency corresponding to the band gap of the $Hg_{0.82}Cd_{0.18}Te$ material is 10.64 THz.

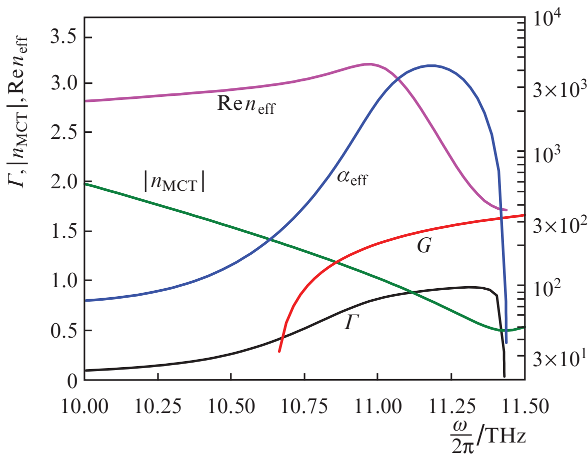

Figure 2. Frequency dependences of the modulus of the refractive index $n_{\rm MCT}$ and the gain G of the $Hg_{0.82}Cd_{0.18}Te$ layer, as well as the real part of the effective refractive index Re$n_{\rm eff}$, the effective absorption coefficient $\alpha_{\rm eff}$, and the optical confinement factor Γ for a hybrid surface plasmon at T = 80 K and $N = 5\times10^{17}$ cm^{-3}.

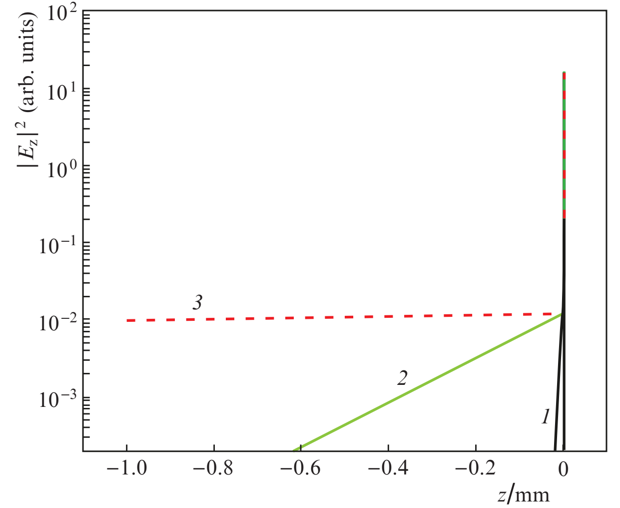

Figure 3. (Colour online) Dependences of the squared modulus E_z on z for a hybrid surface plasmon at frequencies of (*1*) 10, (*2*) 11.435, and (*3*) 11.439 THz, T = 80 K, and $N = 5\times10^{17}$ cm^{-3}.

At a frequency of 11.435 THz, the jump in $|E_z(z)|$ at the CdTe–$Hg_{0.82}Cd_{0.18}Te$ interface (Fig. 4) becomes huge (about 33 times!), because $|n_{\rm CdTe}|/|n_{\rm MCT}|$ = 2.816/0.493; therefore, a significant part of the mode is localised in the active $Hg_{0.82}Cd_{0.18}Te$ layer with a thickness of only 100 nm (Γ = 0.393), although the rest of it begins to penetrate deeply into the GaAs substrate (to a depth of $\sim$0.5 mm, which corresponds to the characteristic thicknesses of the substrates). A slight increase in the frequency (up to 11.439 THz) leads to the fact that, despite an almost imperceptible change in the $|n(z)|$ distribution, the mode is virtually delocalised and the Γ factor decreases to 0.03 (Fig. 5).

Let us consider in more detail the range of frequencies close to the frequency corresponding to the minimum of $|n_{\rm MCT}|$ (Fig. 5), in which there is a sharp decrease in both $\alpha_{\rm eff}$ and Γ. At $N = 5\times10^{17}$cm^{-3} and T = 80 K, the gain G

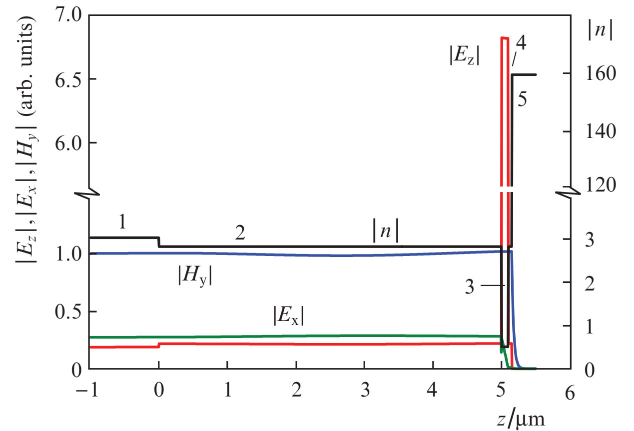

Figure 4. (Colour online) Dependences of the refractive index modulus n, moduli E_z, E_x, and H_y on z for a hybrid surface plasmon on a smaller scale compared to Fig. 3 at a frequency of 11.435 THz for T = 80 K and $N = 5\times10^{17}$ cm^{-3}. The numbers indicate the layers in the structure: (1) GaAs, (2, 4) CdTe, (3) $Hg_{0.82}Cd_{0.18}Te$, and (5) Au.

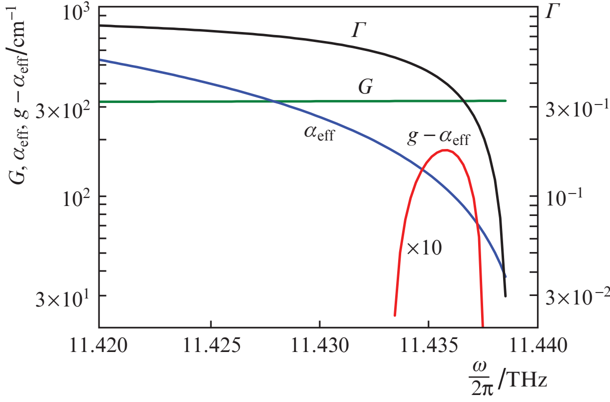

Figure 5. Frequency dependences of the gain G, the optical confinement factor Γ, the absorption coefficient α_{eff}, and the difference between the mode gains g and α_{eff} for a hybrid surface plasmon at T = 80 K and $N = 5 \times 10^{17}$ cm^{-3}.

(~300 cm^{-1}) exceeds α_{eff} at frequencies above 11.428 THz. However, in the frequency range from 11.433 to 11.437 THz, the value of Γ does not decrease as fast as the absorption; therefore, in this range, the difference between the mode gain g and α_{eff} becomes positive and its maximum value $(g-\alpha_{eff})_{max}$ reaches 18 cm^{-1} at the corresponding frequency $\omega_{max}/2\pi$ = 11.326 THz.

Figure 6 shows the dependences $(g-\alpha_{eff})_{max}$, $\omega_{max}/2\pi$ and Γ_{max} (Γ at $\omega = \omega_{max}$) on the concentration of photoexcited carriers in a hybrid surface plasmon. One can see that the difference $(g-\alpha_{eff})_{max}$ becomes positive at $N = 4.8 \times 10^{17}$ cm^{-3}. With increasing N, $(g-\alpha_{eff})_{max}$ shifts to shorter wavelengths and $\omega_{max}/2\pi$ increases almost linearly from 11.25 THz at $N = 4.8 \times 10^{17}$ cm^{-3} to 13 THz at $N = 7.25 \times 10^1$ cm^{-3}. In this case, an increase in both Γ_{max} (from 0.35 to 0.584) and the gain G is observed, which leads to an increase in $(g - \alpha_{eff})_{max}$ to 195 cm^{-1}. Note that to start lasing, it is only necessary to overcome the useful losses on the mirrors, $\alpha_m = (1/L)\ln(1/r)$ [28], where L is the laser cavity length and r is the power reflection coefficient. An approximate expression for r has the form $r = |(n_{eff}-1)|/|(n_{eff}+1)|^2$, which for Re$n_{eff} \approx 1.7$ (see Fig. 2) and L = 3 mm yields $\alpha_m \approx 9$ cm^{-1}. These losses can be overcome already at the threshold concentration $N_{th} = 4.9 \times 10^{17}$ cm^{-3} (Fig. 6).

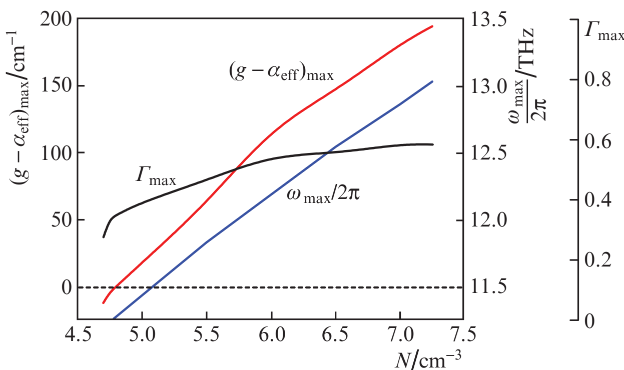

Figure 6. Dependences of $(g - \alpha_{eff})_{max}$, $\omega_{max}/2\pi$, and Γ_{max} on N for a hybrid surface plasmon at T = 80 K.

Let us estimate the threshold pump radiation intensity $I_{th} = \hbar\Omega d R_{th}/\eta$ ($\hbar\Omega$ and η are the quantum energy and the fraction of the pump radiation absorbed in the active layer, respectively; and R_{th} is the rate of recombination of nonequilibrium carriers) required for the generation of stimulated emission from a hybrid surface plasmon to be started.

For the considered carrier concentrations and the $Hg_{0.82}Cd_{0.18}Te$ solid solution, the most efficient recombination mechanism is Auger recombination, which involves two electrons and one hole [19]. In this case, we can assume that $R_{th} \approx C_n N_{th}^3$, where C_n is the Auger recombination coefficient, the value of which for $Hg_{0.82}Cd_{0.18}Te$ at T = 80 K is 1.5×10^{-24} cm^6 s^{-1} [19]. When only the active $Hg_{0.82}Cd_{0.18}Te$ layer (in order to avoid the production of nonequilibrium carriers in the CdTe and GaAs layers, leading to additional absorption of the generated radiation) is pumped through the GaAs substrate by radiation with a wavelength of 2.3 μm ($\hbar\Omega \approx 0.54$ eV) [6], the pump radiation passes twice through the active layer due to almost total reflection from the Au layer, and therefore $\eta = 1 - \exp(-2\alpha_\Omega d)$, where α_Ω is the absorption coefficient of pump radiation in the $Hg_{0.82}Cd_{0.18}Te$ layer. For our case ($\alpha_\Omega \approx 10^4$ cm^{-1} [26] and d = 100 nm), η = 0.18; therefore, $I_{th} \approx 850$ kW cm^{-2}, which is quite achievable under pulsed pumping.

4. Effect of the active region doping on the lasing threshold

The threshold intensity of pump radiation can be reduced by using a technique such as the doping of the active region. As shown earlier [29], donor doping of the active region can lead to a decrease in the Auger recombination rate due to different concentrations of electrons and holes. Indeed, during donor doping of the active region, an additional concentration of free electrons N_d arises, and then it is necessary to replace N by $N + N_d$ in expressions (3) and (6), and the expression for the threshold rate of Auger recombination changes to the following:

$$R_{th} \approx C_n (N_d + N_{th})^2 N_{th}. \quad (10)$$

In this case, N_{th} will significantly decrease from 4.9×10^{17} to 1.55×10^{17} cm^{-3} with an increase in N_d to 7×10^{17} cm^{-3} (Fig. 7). Therefore, according to formula (10), one will

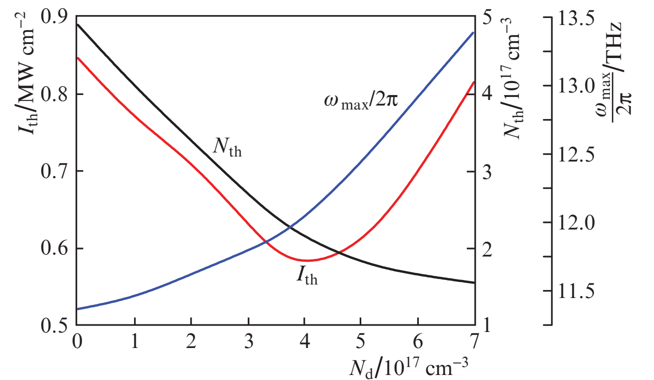

Figure 7. Dependences of I_{th}, N_{th}, and $\omega_{max}/2\pi$ on N_d for a hybrid surface plasmon at T = 80 K.

observe a minimum Auger recombination rate and, hence, a minimum threshold pump radiation intensity I_{th}. Figure 7 shows that a minimum I_{th} is ~570 kW cm^{-2} at N_d = 4×10^{17} cm^{-3} and $N_{th} = 2.2 \times 10^{17}$ cm^{-3}. This means that by choosing the concentration of the donor impurity, it is possible to reduce the lasing threshold by a factor of 1.5. Note also that doping leads to an increase in the frequency ω_{max} at which lasing will occur: $\omega_{max}/2\pi \approx 12$ THz at a minimum I_{th}.

5. Conclusions

Thus, we performed a theoretical study of the possibility of amplifying a hybrid surface plasmon in a structure based on a thin bulk $Hg_{0.82}Cd_{0.18}Te$ layer covered with a metal layer. Due to a dramatic decrease in the modulus of the dielectric constant of the $Hg_{0.82}Cd_{0.18}Te$ layer down to 0.243 at frequencies higher than the frequency corresponding to the band gap of the $Hg_{0.82}Cd_{0.18}Te$ solution, the optical confinement factor of the hybrid surface plasmon was ~0.5, despite the small value (0.0065) of the ratio of the active region thickness to the hybrid surface plasmon wavelength. This can make it possible to observe lasing at a frequency of 11.435 THz at T = 80 K and a threshold concentration of photoexcited carriers of 4.9×10^{17} cm^{-3}. Doping of the $Hg_{0.82}Cd_{0.18}Te$ layer with a donor impurity having a concentration of 4×10^{17} cm^{-3} will lead to a decrease in the threshold concentration of photoexcited carriers down to2.2×10^{17} cm^{-3}, which will reduce the threshold pump radiation intensity from 850 to 570 kW cm^{-2} with an increase in the generation frequency up to 12 THz.

Acknowledgements. This work was supported by the Ministry of Science and Higher Education [Grant No. 075-15-2020-797 (13.1902.21.0024)].

References

1. Vitiello M.S., Scalari G., Williams B., De Natale P. *Opt. Express*, **23**, 5167 (2015).
2. Rogalski A. *Rep. Prog. Phys*., **68**, 2267 (2005).
3. Ushakov D., Afonenko A., Khabibullin R., Ponomarev D., Aleshkin V., Morozov S., Dubinov A. *Opt. Express*, **28**, 25371 (2020).
4. Melngailis I., Strauss A. *Appl. Phys. Lett*., **8**, 179 (1966).
5. Arias J.M., Zandian M., Zucca R., Singh J. *Semicond. Sci. Technol*., **8**, S255 (1993).
6. Morozov S.V., Rumyantsev V.V., Fadeev M.A., Zholudev M.S., Kudryavtsev K.E., Antonov A.V., Kadykov A.M., Dubinov A.A., Mikhailov N.N., Dvoretsky S.A., Gavrilenko V.I. *Appl. Phys. Lett*., **111**, 192101 (2017).
7. Morozov S.V., Rumyantsev V.V., Kadykov A.M., Dubinov A.A., Kudryavtsev K.E., Antonov A.V., Mikhailov N.N., Dvoretskii S.A., Gavrilenko V.I. *Appl. Phys. Lett*., **108**, 092104 (2016).
8. Kudryavtsev K.E., Rumyantsev V.V., Aleshkin V.Ya., Dubinov A.A., Utochkin V.V., Fadeev M.A., Mikhailov N.N., Alymov G., Svintsov D., Gavrilenko V.I., Morozov S.V. *Appl. Phys. Lett*., **117**, 083103 (2020).
9. Fadeev M.A., Dubinov A.A., Aleshkin V.Ya., Rumyantsev V.V., Utochkin V.V., Teppe F., Höubers H.-W., Mikhailov N.N., Dvoretskii S.A., Morozov S.V. *Quantum Electron*., **49**, 556 (2019) [*Kvantovaya Elektron*. **49**, 556 (2019)].
10. Alymov G., Rumyantsev V., Morozov S., Gavrilenko V., Aleshkin V., Svintsov D. *ACS Photonics*, **7**, 98 (2020).
11. Dubinov A.A., Aleshkin V.Ya. *Int. J. High Speed Electron. Syst*., **25**, 1640018 (2016).
12. Kapralov K., Alymov G., Svintsov D., Dubinov A. *J. Phys. Condens. Matter*, **32**, 065301 (2020).
13. Lobet M., Liberal I., Knall E.N., et al. *ACS Photonics*, **7**, 1965 (2020).
14. Zhong Y., Malagari S.D., Hamilton T., Wasserman D. *J. Nanophotonics*, **9**, 093791 (2015).
15. Oulton R.F., Sorger V.J., Genov D.A., Pile D.F.P., Zhang X. *Nat. Photonics*, **2**, 496 (2008).
16. Berini P., De Leon I. *Nat. Photonics*, **6**, 16 (2012).
17. Bachmann F., Loosen P., Poprawe R. *High Power Diode Lasers. Technology and Applications* (New York: Springer Science–Business Media, 2007).
18. Moazzami K., Phillips J., Lee D., Krishnamurthy S., Benoit G., Fink Y., Tiwald T. *J. Electron. Mater*., **34**, 773 (2005).
19. Chu J., Sher A. *Physics and Properties of Narrow Gap Semiconductors* (New York: Springer Science–Business Media, 2008).
20. Krishnamurthy S., Sher A. *J. Appl. Phys*., **75**, 7904 (1994).
21. Shkerdin G., Stiens J., Vounckx R. *J. Appl. Phys*., **85**, 3792 (1999).
22. Ferrini R., Guizzetti G., Patrini M., Parisini A., Tarricone L., Valenti B. *Eur. Phys. J. B*, **27**, 449 (2002).
23. Talwar D.N., Yang T.-R., Feng Z.C., Becla P. *Phys. Rev. B*, **84**, 174203 (2011).
24. Palik E.D. *Handbook of Optical Constants of Solids* (Orlando: Academic Press, 1985).
25. Dvoretsky S., Mikhailov N., Remesnik V., Sidorov Y., Shvets V., Ikusov D., Varavin V., Yakushev M., Gumenjuk-Sichevska J., Golenkov A., Lysiuk I., Tsybrii Z., Shevchik-Shekera A., Sizov F., Latyshev A., Aseev A. *Opto-Electron. Rev*., **27**, 282 (2019).
26. Daraselia M., Carmody M., Edwall D.D., Tiwald T.E. *J. Electron. Mater*., **34**, 762 (2005).
27. Landau L.D., Lifshits E.M. *Electrodynamics of Continuous Media* (Oxford: Pergamon Press, 1960; Moscow: Nauka, 1989).
28. Casey H.C., Panich M.B. *Heterostructure Lasers* (New York: Academic Press, 1978).
29. Dubinov A.A., Aleshkin V.Ya., Morozov S.V. *Semiconductors*, **52**, 1221 (2018) [*Fiz. Tekh. Poluprovodn*., **52**, 1100 (2018)].